This article must be cited as:

Cristian Lupan,[1,*] Rasoul Khaledialidusti,[2] Abhishek Kumar Mishra,[3,*,‡] Vasile Postica,[1,‡] Maik-Ivo Terasa,[4] Nicolae Magariu,[1] Thierry Pauporté,[5,*] Bruno Viana,[5] Jonas Drewes,[6] Alexander Vahl,[6] Franz Faupel,[6] Rainer Adelung [4,*]

Pd-Functionalized ZnO:Eu Columnar Films for Room Temperature Hydrogen Gas Sensing: A Combined Experimental and Computational Approach

ACS Appl. Mater. Interfaces 2020, 12, 24951−24964. DOI: 10.1021/acsami.0c02103

1 *Center for Nanotechnology and Nanosensors, Department of Microelectronics and Biomedical Engineering, Technical University of Moldova, 168, Stefan cel Mare Av., MD-2004, Chisinau, Republic of Moldova*

2 *Department of Mechanical and Industrial Engineering, Norwegian University of Science and Technology (NTNU), 7491, Trondheim, Norway*

3 *Department of Physics, School of Engineering, University of Petroleum & Energy Studies, Bidholi via Premnagar, Dehradun, 248007, India*

4 *Functional Nanomaterials, Faculty of Engineering, Institute for Materials Science, Kiel University, Kaiserstr. 2, D-24143, Kiel, Germany*

5 *PSL Université, Chimie ParisTech, CNRS, Institut de Recherche de Chimie Paris (IRCP), 11 rue P. et M. Curie, F, 75005 Paris, France*

6 *Chair for Multicomponent Materials, Faculty of Engineering, Institute for Materials Science, Kiel University, Kaiserstr. 2, D-24143, Kiel, Germany*

*Corresponding authors:

Prof. Dr. Thierry Pauporté (thierry.pauporte@chimieparistech.psl.eu)
PSL University, CNRS, France

Prof. Dr. R. Adelung (ra@tf.uni-kiel.de)
Kiel University, Germany

Prof. Dr. Abhishek K. Mishra (akmishra@ddn.upes.ac.in)
University of Petroleum and Energy Studies, India

C. Lupan (cristian.lupan@mib.utm.md)
Technical University of Moldova, Republic of Moldova

KEYWORDS: Eu-doped ZnO, gas sensor, Pd, hydrogen, chemical deposition, DFT, functionalization.

ABSTRACT

Reducing the operating temperature to room temperature is a serious obstacle on long-life sensitivity with long-term stability performances of gas sensors based on semiconducting oxides and this should be overcome by new nano-technological approaches. In this work, we report the structural, morphological, chemical, optical and gas detection characteristics of Eu-doped ZnO (ZnO:Eu) columnar films as a function of Eu content. The scanning electron microscopy (SEM) investigations showed that columnar films, grown via synthesis from chemical solutions (SCS) approach, are composed of densely packed columnar type grains. The sample sets with a content of ~0.05, 0.1, 0.15 and 0.2 at% of Eu in ZnO:Eu columnar films were studied. The surface functionalization was achieved using $PdCl_2$ aqueous solution with additional thermal annealing in air at 650 ºC. The temperature dependent gas-detection characteristics of Pd-functionalized ZnO:Eu columnar films were measured in detail, showing a good selectivity towards H_2 gas at operating OPT temperatures of 200 – 300 ºC among several test gases and volatile organic compounds (VOCs) vapors; such as methane, ammonia, acetone, ethanol, *n*-butanol and 2-propanol. At an operating temperature OPT of 250 ºC a high gas response I_{gas}/I_{air} ~ 115 for 100 ppm H_2 was obtained. Experimental results indicate that Eu-doping with an optimal content about 0.05 – 0.1 at% along with Pd-functionalization of ZnO columns leads to a reduction of the operating temperature of the H_2 gas sensor. DFT based computations provide mechanistic insights into the gas sensing mechanism by investigating interactions between the Pd-functionalized ZnO:Eu surface and H_2 gas molecules supporting the experimentally observed results. The proposed columnar materials and gas sensor structures would provide a special advantage in the fields of fundamental research, applied physics studies, ecological and industrial applications.

1. INTRODUCTION

One of the great challenges in stability and long-term detection of gas sensors based on semiconducting oxides is to reduce the operating temperature, specifically to the room temperature and this should be overcome by new nano-technological methods. Hybrid nano-materials, including new 2D materials [1–6], metal oxides [7–10] and other metallic systems [11] have shown exceptional promise for gas detecting and catalytic applications. Doping is an important procedure to control the sensor response with atomic surface arrangement as well as active adsorption sites for targeted gas, which are intentionally produced by doping foreign atoms in the oxides. In this context, doping of semiconducting/metal oxide nano- and microstructures with various rare earth (RE) elements, such as Tb, Er, Ce, La, Eu, etc. [1,12,13], becomes very important for improving the optical and electrical properties. This is fascinating for gas sensing applications as well due to their fast oxygen ion mobility, effective catalytic nature, and high surface basicity of the RE–based materials [1,14,15]. For instance, Xu and Yan fabricated a new fluorescent sensor based on Eu^{3+}-functionalized ZnO at metal–organic frameworks for volatile aldehyde gases (acetaldehyde, acraldehyde and formaldehyde) detection in ppb range at room temperature [16]. Somacescu *et al.* successfully synthesized binary $ZnO–xEu_2O_3$ (x = 5 wt%) oxide through a hydrothermal route demonstrating a high sensor signal down to 3 ppm of NO_2 gas, as well as a low sensitivity towards CO gas [2].

In this context, zinc oxide which corresponds to II and VI group semiconducting oxide material with a large bandgap (~3.37 eV, at room temperature (RT)) crystallizes in its hexagonal wurtzite phase as the most popular structure due to its stability at RT and this makes it an attractive material for doping with RE elements. However, the efficient adding of RE^{3+} ions into the ZnO lattice is challenging due to different technological approaches used, the large differences in ionic radii of

RE^{3+} ions ($r(Eu^{3+})$= 95 pm) and Zn^{2+} ions ($r(Zn^{2+})$= 74 pm) [17] and also due to the low solubility limit of the impurities [18]. The clear evidence of ZnO nano- and microstructures doping with rare earth ions was observed in the case of synthesis using chemical methods [19], electrodeposition [12], hydrothermal synthesis [20], ion implantation [18], etc.. In this context, chemical synthesis from the solution (SCS) allows the doping with ions of different metals, including RE elements, during the growth process by introducing salts in the complex solution [21], and SCS has been used in the present study for growth of Eu-doped ZnO columnar films with a concentration of up to 0.2 at% Eu.

Among all RE elements, europium has attracted a great attention due to its outstanding optical properties [1,12,13]. Eu^{3+} ions are highly stable, biocompatible and thus are attractive luminescence centers where electronic transitions between 4*f* levels ($^5D_0$-$^7F_2$ transition) can generate intense emission lines [12,22]. The RE ions, especially Ln^{3+}, possess numerous transition bands which are close to each other, and are conducive to population exchange creating a thermal equilibrium among them. The successful inclusion of Eu^{3+} ions in the crystalline network of ZnO and the creation of new energy levels were reported by only few authors [1,14], showing high interest to achieve control of electrical conductivity for sensor applications as well, since such Ln^{3+} ions are stable, thus could be used in a wide working temperature range. For example, Zhou *et al.* prepared hybrid nanostructures on Eu-decorated ZnO quantum dots for radiometric detection of *Bacilus anthracis* spores [23]. Likewise, Pd is also known as one of the most extensively applied catalytic materials that can lower the operating temperature for maximum response of gas sensors based on semiconducting metal oxide nano- and microstructures [24].

Therefore, based on a synergistic effect of both Eu and Pd elements [12,25], the aim of this work is to design the higher performance gas sensors on Pd-functionalized ZnO:Eu columnar films

synthesized by the SCS method and also to reduce the operating temperature of the sensor. The surface functionalization of ZnO:Eu columnar films with Pd nanoparticles was carry out following the previously reported technique based on $PdCl_2$ aqueous solutions [26]. The morphological, chemical, optical and gas sensing properties are reported in detail. Density functional theory (DFT) based calculations provide detailed understanding into the sensing mechanism by investigating interactions between the Pd_n:Eu: ZnO $(10\bar{1}0)$ surface and H_2 gas molecules. Further improvements can be achieved by changing synthesis parameters and control concentration of ions of Eu in columnar films of ZnO:Eu, which can lead to higher response, rapid recovery times, and lower operating temperature.

2. EXPERIMENTAL AND COMPUTATIONAL DETAILS

2.1. Growth of ZnO:Eu columnar films.

The Eu-doped ZnO columnar films, with thicknesses of 1.3 – 1.5 µm (investigated in cross-section using SEM, see **Figure S1**), were synthesized with help of a SCS approach from aqueous baths (at temperatures around 90 ºC), as reported in previous works [9,21,26]. As substrate, the commercial glass slides were used with pre-cleaning and sensitization, according to the procedure reported previously [26]. To achieve 0.05, 0.1, 0.15 and 0.2 at% of Eu in ZnO:Eu columnar films (measured using EDX and noted as Eu1, Eu2, Eu3 and Eu4, respectively), see Supporting Information, the 10, 20, 30 and 40 mM of $EuCl_3$ were respectively added in the complex solution. To increase the crystallinity of as-grown films, a thermal annealing (TA) in air at 450, 550 or 650 ºC for 120 min was applied. Also, the rapid thermal annealing (RTA) in air at 450, 550 or 650 ºC for 1 min was done on some sample sets used for improving structures in order to decrease the thermal budget for sensor fabrication. The surface functionalization of ZnO:Eu columnar films

with palladium nanoparticles was accomplished following the previously reported approach based on $PdCl_2$ aqueous solutions followed by TA-treatment [26].

2.2. Characterization of material.

The morphology of the specimens was investigated using a scanning electron microscope (SEM) (Zeiss Supra 55VP) operated at 7 kV (10 µA). To find the origin of the columnar structures monitored in the SEM images for all samples, compositional SEM images were created by mapping analysis with energy dispersive X-ray (EDX, Zeiss Supra 55VP) at microstructural level. In order to investigate the chemical composition, four europium doped columnar ZnO thin films (ZnO:Eu) with different Eu doping concentrations were investigated by energy dispersive X-ray (EDX; Zeiss Supra 555VP, 15 kV) analysis and by X-ray photoelectron spectroscopy (XPS with Omicron Nano-Technology GmbH, Al-anode, 240W). All recorded spectra were charged referenced by calibrating the line C-1s of advantageous carbon at 285.0 eV [27]. For the analysis of XPS spectra the software CasaXPS (version, 2.3.16) was used. The gas sensing tests and measuring apparatus were same as reported in our papers [24,26]. The two-point probe approach was involved for the electrical current study of undoped and Eu-doped zinc oxide nanocolumnar layers, annealed at diverse regimes by using two methods (TA and RTA). The concentration of test gases was determined according to the chamber volume considering the densities of the liquid VOCs. By monitoring the electrical current value through the columnar ZnO:Eu-based sensor, the electrical conductance was investigated in air and in a test species. The operating temperature was first set at room temperature (RT), and then varied from 150 to 350 ºC with a 50 ºC step, in order to investigate the influence of this parameter on the gas sensing properties of the developed samples. No gas response at RT, or a temperature lower than 150 ºC was observed for as-grown samples. The gas response (S) was determined using the $S = I_{gas}/I_{air}$ ratio, where I_{gas} is the electrical

current through the sample when gas was introduced into the chamber with sensor, and I_{air} is the electrical current at the exposure in air. The response time (τ_r) is defined as the period needed for the sensor to reach 90% of saturation electrical conductivity from 10% of initial value, while the recovery time (τ_d) is definite as the time taken for saturation current to reach 10% of its saturation current value after stopping introduction of gas into the test chamber [24,26].

2.3. Computational details.

First-principles calculations based on the DFT-density functional theory were performed using the generalized gradient approximation with the PBE-Perdue–Burke–Ernzerhof [28] exchange–correlation functional and the projected augmented wave (PAW) [29] approach with a plane wave cutoff energy of 520 eV, as implemented in the VASP - Vienna *ab initio* Simulation Package [30]. The atomic positions and lattice constants were fully optimized using conjugate gradient approach until the maximum residual force acting on each atom became less than 0.0001 eV/Å. Energy convergence criterion employed was 10^{-7} eV/cell. For the unit cell of ZnO bulk, 5×5× 4 MP-Monkhorst-Pack *k* points were used [31]. The ZnO ($10\bar{1}0$) surfaces were modelled using the 5×4×1 MP-Monkhorst-Pack *k* points. The partial occupancies were determined using the MP-Methfessel–Paxton smearing scheme [32] with smearing width off 0.1 eV. A large vacuum space with a thickness of at least 20 Å was used to avoid any interaction between a ZnO ($10\bar{1}0$) and its periodic images along the *c*-axis. As long-range dispersion forces are necessary for the accurate description of the surfaces interactions with the adsorbate molecules, we used the Grimme's method for the incorporation of van der Waals interaction (DFT-D2) [33]. We did not include the Coulomb effect (U) for the localized 3d electrons of metal atoms because of their negligible effect on the results in our case. The surface energies of the relaxed slabs were found using a combination

of calculations for the relaxed and unrelaxed surfaces as given in SI (**Figure S2**). Bader charges were calculated using a developed by Henkelman and co-workers [34].

3. RESULTS AND DISCUSSION

3.1. Morphological and structural properties.

Figure 1(a-c) and **1(d-f)** shows the SEM images of as-grown ZnO:Eu columnar films with 0.05 and 0.2 at% Eu, respectively. Specimens are formed of well-packed columnar-type grains, which absolutely completely cover the glass sensor substrate. Formation of agglomerations or presences of holes were not observed for ZnO with low content of Eu, i.e. about 0.05 at%. (see **Figure 1(a)**). However, the formation of low-density agglomerations can be observed as Eu content increases (about 0.2 at%, see **Figure (1d)**). This can be explained based on the segregation of Eu at the top surface due to the limited solubility of Eu in ZnO [35,36]. The SEM images of TA-treated samples at 650 ºC for 2 h and with different content of Eu (about 0.1, 0.15 and 0.2 at%) are presented in **Figures 1(g)-1(i)**. **Figures 1(j)-1(l)** present the SEM images of Pd-functionalized ZnO:Eu columnar films. On the surface of ZnO:Eu grains, a distribution of nanoparticles with diameter of 5 – 15 nm and a high lateral density of ~ 8×10^8 cm^{-2} (estimated from SEM images) can be observed. Such a large distribution in the diameter of nanoparticles can be a result of coalescence during thermal annealing [37]. However, the formation of percolating paths based on nanoparticles was not observed (see **Figures 1(k)** and **1(l)**). Compositional images taken by energy dispersive EDX elemental mapping at the micro-structural level of columnar ZnO:Eu2 with ~0.1 at% Eu films, thermally annealed at 650 ºC for 2 h is shown in **Figure S2**.

Nanostructured semiconducting/metal oxide films with controlled surface area, grain sizes, and crystal morphologies are convenient for many applications, including gas sensing, which allows the efficient control of surface activity [38]. In order to evaluate the influence of Eu content and effects of TA treatments on grain diameter, we report the grain diameter distribution of studied samples (measured from SEM images) in **Figure 2**. From **Figure 2a** it can be observed that by increasing the Eu content in as-grown ZnO:Eu columnar films, the grain diameter decreases from 275 – 425 nm to 200 – 350 nm. The decrease in the grain diameter was also observed in TA-treated samples with increasing Eu content (see **Figure 2(c-d)**). The decrease in grain size by Eu doping has been observed by other authors [20,22] as well, and can be due to the existence of Eu^{3+} ions in complex solution which acts as crystal growth inhibitors [39]. The increase in grain diameter after TA treatment indicates the generation of more activation energy for the growth of bigger columns-grains, which is in accordance with other work [40].

Figure 3a shows the position of XRD diffraction (1 0 $\bar{1}$ 0), (0 0 0 2) and (1 0 $\bar{1}$ 1) peaks and intensity for ZnO and ZnO:Eu (Eu4 with 0.2 at% Eu) columnar films, in order to demonstrate the slight shift (~ 0.3º) to the lower values of 2θ after doping with Eu. This can be ascribed to doping with larger Eu^{3+} cations (effective ionic radius 0.95 Å) than Zn^{2+} (of 0.74 Å) and induce an expansion of the zinc oxide unit cell volume (by substitution of Eu^{3+} ions at the Zn^{2+} sites [20,22]). Earlier, using *ab initio* density functional theory DFT methods supported on generalized gradient approximation, it was established that Eu ions can substitute favorably Zn sites in the zinc oxide host lattice [25]. The decrease in intensity of (1 0 $\bar{1}$ 0) and (1 0 $\bar{1}$ 1) peaks after Eu-doping shows that the preferential growth of ZnO columnar films was strongly affected, giving rise to the (0 0 0 2) orientation and to the growth of ZnO grains with smaller diameter (as was observed from SEM images, see **Figures 1** and **2**). This can be interpreted based on the presence of Eu^{3+} ions in the

complex solution which acts as crystal growth inhibitors, especially for (1 0 $\bar{1}$ 0) and (1 0 $\bar{1}$ 1) orientations, by decreasing the free energy of surface in (0 0 0 2) direction [39,41]. For more details, various parameters which describe structural characteristics of the samples were calculated as was reported recently [21] and presented in **Table 1**. The slight changes in the lattice parameters can be observed after doping with Eu. For example, *a* and *c* increased from 3.250 and 5.211 Å to 3.256 and 5.251 Å, respectively. A slight increase of the average crystallite size was also observed (from 5.25 to 6.58 nm). The increased residual stress also indicates the expansion of the zinc oxide unit cell volume after Eu^{3+} doping [20,22]. Dislocation densities (δ) are measured using the relation $\delta = 1/d^2$ and exhibit a decrease when doped with Eu, which indicates lower concentration of lattice imperfections [42].

Figure 3b shows the XRD pattern of Pd-functionalized ZnO:Eu columnar film with deposited Au contacts. The peaks notated with a hashmark (#) match adequately the gold face center cubic (fcc) (Au, JCPDS Files Card # 04-9748), and can be attributed to the gold electrical contacts on the surface of ZnO:Eu columnar film for further external connections. Remaining peaks can be assigned to wurtzite ZnO (JCPDS Files Card # 36-1451). No secondary phases or impurities of the Eu and Pd or their oxides (for example Eu_2O_3 or PdO) were found due to detection limit, indicating that Eu ions did not modify fundamentally the crystal structure and that doping concentration of Eu in ZnO is lower than the solubility limit [35]. In the literature, it has been shown that when the doping concentration is high, impurity phases of oxides were observed. For example, Che *et al.* observed the formation of Eu_2O_3 in $Zn_{1-x}Eu_xO$ films for doping concentrations around 20%, which is much higher than our films [35]. Kumar *et al.* observed an additional small peak at 29.4º for $ZnO:Eu^{3+}$ nanophosphors, which was attributed to Eu_2O_3 phase (JCPDS File Card No. 43-1009),

but only at high Eu^{3+} concentrations (6 mol%) [22]. In our samples, the Pd or its oxides were not detected due to low XRD instrumental detection limit.

Table 1. Structural parameters of undoped and Eu-doped ZnO layers deposited by SCS

Eu content and type of treatment	XRD (002) peak position (2θ°)	FWHM for (002) peak (°)	The average crystallite size D (nm)	d (002), (Å)	a (100), (Å)	c (002), (Å)	Residual stress through *c*-axis σ (Pa)	Dislocation density δ (x 10^{14} line/m²)
un-doped, TA650	34.42	0.36	5.25	2.605	3.250	5.211	-0.409	0.0362
ZnO:Eu2, ~0.1at%, TA650	34.12	0.232	6.58	2.625	3.256	5.251	-2.001	0.0191

3.2. Chemical and optical properties.

The overview XPS spectrum corresponding to a ZnO:Eu thin film with 0.05 at% Eu-doping is shown in **Figure 4a**. The overview spectrum reveals the existence of signal corresponding to the elements Zn, O and C, while due to the low doping concentration no characteristic peaks for Eu can be observed in this sample set. Accordingly, for comparison, also two thin film samples with significantly higher Eu-doping concentrations were investigated and the Eu characteristic peaks were observed, as depicted at the example of high-resolution spectra of the Eu-3d lines (see **Figure S3**). The peak location of the Eu-3d lines gives strong indication that Europium is present as Eu^{3+} in the columnar ZnO:Eu thin films. The closer evaluation of the Zn-2p lines (**Figure 4b**)

yields information about the oxidation state of Zn in the ZnO:Eu thin films. As depicted in **Figure 4b**, the Zn-$2p_{3/2}$ line is located with a peak around 1022.5 eV, which corresponds well with Zn^{2+} in ZnO (commonly reported between 1021.4 eV and 1022.5 eV) [43]. Interestingly, for the thin films prepared at significantly higher Eu concentration, the peak position of the Zn-$2p_{3/2}$ line is shifted slightly towards lower binding energies (around 1021.7 eV), which is still in well agreement with Zn^{2+} in ZnO. This can be explained based on the electrical charge transfer between Eu^{3+} and Zn^{2+} and the change of electronic structure of Zn, due to doping of ZnO columnar films with Eu and the small energy shift could result in the modification of electric field of Zn^{2+} as well as an increase of the electron density, and hence a small decrease of the binding energy of Zn^{2+} ions [44–46]. XPS measurements integrated with XRD results and optical features presented in the following part corroborate that Eu^{3+} have been introduced as dopant into the ZnO columnar films lattice [44,45].

Figure 5a shows the optical transmittance spectra of specimens, namely as-grown ZnO:Eu columnar films with different contents of Eu, to study the influence of Eu content on the optical characteristics of ZnO:Eu columnar films. The columnar films exhibit a good transparency in the visible range and a steep rise at the absorption optical edge. One can see that the spectra of ZnO:Eu sample sets are the characteristic of zinc oxide phase [12,47]. **Figure 5b** shows the optical transmittance spectra of ZnO:Eu columnar films with about 0.15 at% Eu treated TA at different temperatures (450, 550 and 650 ºC) for 2 h. For all specimens the optical transmittance in the visible region is higher than 60%, while the sharp band in the UV cut-off range was found around 380 - 390 nm, which can be attributed to the band-to-band transition of ZnO [22]. Two tendencies were observed, namely, the decrease in the optical transmittance by Eu-doped ZnO columnar films up to 0.15 at% (see **Figure 5a**) and the increase in the optical transmittance of ZnO:Eu columnar films with a raise in TA treatment temperature from 450 to 650 ºC (see **Figure 5b**). The decrease

in the optical transmittance of ZnO:Eu nanoparticles by increase in Eu content was also observed by Pessoni *et al.* [48] and Koao *et al.* [49], because of the increase in strain and the deterioration of the crystalline quality [48,49]. The increase in the optical transmittance by increasing in the temperature of TA treatment can be attributed to the slight change in grain size, namely the increase in grain mean diameter with Eu content increase [50,51], which was observed by SEM data and related to crystallinity changes.

The optical band gap (E_g) of the europium-doped zinc oxide nanocolumnar films was evaluated by the extrapolation of the linear portion of $(\alpha h\nu)^2$ versus $h\nu$ plots, assuming the direct transitions for ZnO in Tauc equation [47], where α is the coefficient of absorption and $h\nu$ is the energy of incident photon. **Figure 5c** shows the plot for the as-grown ZnO:Eu columnar layers with different Eu contents, while **Figure 5d** shows the plot for ZnO:Eu columnar films with about 0.15 at% Eu TA-treated at different temperatures for 2 h. While the increase in Eu content in films do not change essentially the value of optical band gap, the increase in TA treatment temperature leads to decrease in the value of E_g from 3.311 eV for as-grown columnar films to 3.25, 3.25 and 3.23 eV for those TA-annealed at 450, 550 and 650 ºC, respectively (see **Figure 5d**). The same tendency was observed for single ZnO crystallite forming films [47], for Sn-doped ZnO columnar films synthesized by the same SCS method [50], and can be explained on a reduced density of defects (namely, annealing of extrinsic and intrinsic defects by TA treatment) and a slight increase in diameters of the crystallites, which was observed by SEM [47,51].

Figure 6a shows the room temperature photoluminescence PL spectra of as-grown ZnO:Eu columnar films with different contents of dopant. This technique can ensure useful data related to defect states and crystallinity of the samples, which is extremely important for H_2 gas sensing applications [50]. The laser excitation wavelength was 266 nm and the line at 532 nm is due to the

second order of the laser related to the grating and excitation wavelength selection. All as-grown samples shown a broad (NBE) near-band-edge emission at ~371 nm with lower intensity compared to deep level emission (DLE) from visible region, which are assigned to intrinsic point defects and defect complexes in ZnO [52]. The same results were observed for Aluminum-doped ZnO (ZnO:Al) layers grown by chemical bath deposition [53], and also ZnO:Eu columnar films [9], and indicate poor crystallinity of as-grown ZnO:Eu columnar films and the presence of high concentration of defects due to low temperature synthesis (about 90 ºC) and stoichiometry with presence of hydroxyl complexes [47,50]. However, from **Figure 6a** it can be observed that with the Eu content increasing in ZnO:Eu columnar films, the intensity of NBE emission is gradually increasing, while the intensity of DLE from visible region is decreasing. This may point out on an increase of crystallinity of ZnO:Eu columnar films by increasing the content of Eu. Therefore, the calculated ratio of NBE and DLE intensity ratio (I_{NBE}/I_{DLE}) is increasing from 0.05 for ZnO to 0.06, 0.25 and 2.55 for ZnO:Eu with about 0.05, 0.1 and 0.15 at% Eu, respectively.

Figure 6b shows the PL spectra of ZnO:Eu columnar films with about 0.1 at% Eu (noted as Eu2) after TA treatment at different temperatures. As can be observed, that for all treated samples the spectra are dominated by the NBE emission at ~370 nm. In this case the I_{NBE}/I_{DLE} ratio is considerably increased to 1.3 and 13 for TA at 450 and 550 ºC, respectively. This indicates an increased crystallinity of ZnO:Eu columnar films after TA, which was also reported by other authors and could be easily explained based on improved stoichiometry [12,47,50,53]. **Figure 6c** shows the visible emission spectrum at room temperature under pumping at 466 nm. At this wavelength corresponding to Eu absorption band, the observed broad peaks at 530 nm can be assigned to ZnO defects as well as to the 5d–4f Eu^{2+} emission [12]. Furthermore, at this excitation wavelength one can also notice peaks which can be attributed to characteristic emission lines of Eu^{3+}. [13]. The Eu^{3+}

f–f transitions peaks are observed at 570, 590, 610, 660 and 690 nm corresponding to the $^5D_0 \rightarrow {}^7F_0$; $^5D_0 \rightarrow {}^7F_1$; $^5D_0 \rightarrow {}^7F_2$; $^5D_0 \rightarrow {}^7F_3$ and $^5D_0 \rightarrow {}^7F_4$, respectively [12,13], but the intensity is relatively low revealing energy transfer between the host matrix and Eu^{3+} dopants.

3.3. DFT study of H_2 gas interaction on Pd-functionalized and Eu- doped ZnO$(10\bar{1}0)$ *surface.*

We first relaxed the unit cell of bulk ZnO structure (see **Figure S4**) and optimized lattice parameters of $a = b = 3.1957$ Å, $c = 5.1437$ Å, $\alpha = \beta = 90^o$, and $\gamma = 120^o$ were obtained, which matches well with the experimental findings of Sawada *et al*. [54] ($a = b = 3.2490$ Å, $c = 5.2052$ Å, $\alpha = \beta = 90^o$, and $\gamma = 120^o$). Our calculated c/a ratio is in 0.01 units with experimental values and the lattice parameters obtained are in good agreement with earlier computations of Jaffe *et al*. employing a Hartree-Fock approach [55] and also with computational results of Cook *et al*. ($a = b = 3.19591$ Å, $c = 5.15851$ Å, $\alpha = \beta = 90^o$, and $\gamma = 120^o$) [56]. Next, we investigated the structure of $(10\bar{1}0)$ surfaces and similarly to earlier works, [56,57] we also found two different possible surface terminations (lattice parameters of $a = 3.2552$ Å; b=5.2396 Å) as shown in **Figure S5**. We considered a total of 6 atomic layers in our slab model, where bottom four layers coordinates were kept frozen at their bulk positions. Through calculated surface energies of these two surface terminations (Termination_I: 2.84 $J.m^{-2}$; Termination_II: 1.12 $J.m^{-2}$), we found Termination_II to be more stable than the other one, which is in agreement with previously published results [56,57].

As a next step and in order to model Eu-doped surfaces, we considered 3×2 supercells including 72 Zn atoms and 72 O atoms, as shown in **Figure S5.** We doped the Eu atoms in four different possible places on the first two atomic layers (see **Figure 7**). DFT calculated ground-

state electronic energies indicate that most stable structure is the one in which we doped Eu atom in the first atomic layer, substituting most exposed Zn atom (**Figure 7a**).

We further tried to adsorb small Pd_n clusters (n = 1 to 9) on the most stable surface termination with Eu dopant, as shown in **Figure S6**. Results indicate that the adsorption energy of the cluster increases with increasing Pd cluster size [**Table S1**], which is similar to works by Lupan *et. al.* [58], where through DFT calculations they found that larger Pd*n* cluster shows stronger adsorption energy on ZnO surface. The stronger bindings for larger clusters are results of large spread over the ZnO surface, which also leads to a greater number of possible bonds between palladium and surface atoms. Pd was found to bind through bridge sites that are in-between Pd and O atoms for both Pd1 and Pd2 clusters, however for larger clusters, hollow sites were found to be populated, leading to a hexagonal close packed (*hcp*) motif on top of the ZnO substrate (see **Figure S6**). To further model the H_2 gas molecule interaction, we choose the Pd5 cluster and placed H_2 molecule over different sites. Results have shown H_2 molecule adsorbed on the surface with the adsorption energy of -0.9099 eV, as presented in **Figure 8**.

In order to analyze the H_2 gas sensing, we investigated partial density of states of the system and also estimated the charge transfer. We note that a negative charge of -0.10 is transferred over the H_2 molecule due to interaction of Pd cluster over Eu: ZnO($10\bar{1}0$) surface (see **Figure 9a**). This is also reflected in terms of Fermi energy change, as Fermi energy changes from -1.0916 for Pd_5:Eu: ZnO($10\bar{1}0$) surface to -1.1470 for H_2 molecule adsorbed over this surface.

3.4. Gas sensing properties on Pd-functionalized and Eu-doped ZnO columnar films.

The gas detection properties were measured for ZnO:Eu and Pd-functionalized ZnO:Eu columnar films with different contents of Eu (0.0 at% - Eu0, ~0.05 at% - Eu1, ~0.1 at% - Eu2,

~0.15 at% - Eu3, ~0.2 at% - Eu4) and TA-treated (T650) or rapidly RTA-treated (R650) at 650 ºC for 120 min or 1 min, respectively. The obtained results are showed in **Figure S7** for ZnO:Eu samples and in **Figure 10** for Pd-functionalized ZnO:Eu columnar film-based samples. The studied samples were noted as: Eu1R650 – ~0.05 at% Eu RTA-treated at 650 ºC for 60 s; Eu4R650 – ~0.2 at% Eu RTA-treated at 650 ºC for 60 s; Eu1T650 – ~0.05 at% Eu TA-treated at 650 ºC for 2 h; Eu4T650 – ~0.2 at% Eu TA-treated at 650 ºC for 2 h.

The gas response of pristine ZnO:Eu columnar films with different contents of Eu to 100 ppm of different gases at working temperature of 350 ºC is presented in **Figure S7a** for samples treated RTA-treated at 650 ºC and in **Figure S7b** for samples TA-treated at 650 ºC. All samples showed a higher gas response to VOC vapors, such as acetone, *n*-butanol, ethanol and 2-propanol, compared to hydrogen, methane and ammonia gases. However, the gas response is relatively low (maximum gas response of ~ 2), thus these samples present no interest for application in highly sensitive and selective gas detection/sensing.

Figure 10a shows the gas response of ZnO:Eu columnar films functionalized with Pd to different gases (hydrogen, methane) and vapors (acetone, *n*-butanol, ethanol, ammonia, 2-propanol) at an operating temperatures of 250 ºC. The concentration of all used gases was 100 ppm for all tests. The H_2 gas response of Pd-functionalized ZnO:Eu columnar films to 100 ppm hydrogen, namely samples noted as Eu1R650(~0.05 at% Eu), is quite high (I_{gas}/I_{air} > 115) and selective. Similar effect was observed for sample sets Eu4R650(~0.2 at% Eu), however H_2 gas response was one order lower (~ 19) compared to Eu1R650 (~ 115), but still quite selective versus all investigated test gases. **Figure S8** shows the dynamic response of Pd-functionalized ZnO:Eu columnar films for 100, 200 and 300 ppm of hydrogen gas measured at room temperature. It is clearly seen sensor effect for these samples at RT. Previous gas sensing studies of ZnO columnar

films [21], as well as the present study of Eu-doped ZnO columnar films, presented no room temperature gas response (see **Figure S7 and Figure 10(b)**). Therefore, the results from **Figure S8(a-c)** demonstrates that Pd-functionalization of ZnO:Eu columnar films can decrease the working temperature for detection of H_2 gas down to room temperature. It was also demonstrated for the Pd-functionalized ZnO:Pd columnar films [26].

All sample sets indicated excellent selectivity to hydrogen gas in an operating temperature range of 200 – 300 ºC (see **Figure 10(a-b)**). As an example, the dependence of the gas response on the operating temperature for Pd-functionalized ZnO:Eu columnar films (~0.05 at% Eu) RTA-treated at 650 ºC (for 60 s) is presented in **Figure 10(b)**. The highest gas response of ~ 115 to 100 ppm of hydrogen gas was obtained at working temperatures around 250 ºC for this type of samples (Eu1R650), which were RTA-treated at 650 ºC for 1 min only. The gas response to hydrogen gas for other sample sets, i.e. Eu4R650, Eu1T650 and Eu4T650 is ~ 19, ~ 13 and ~ 8, respectively. The highest gas response of samples with ~0.05 at% Eu compared to higher concentrations of Eu-doped samples can be explained based on amorphous Eu_2O_3 segregation at the grain boundary of ZnO:Eu columnar films by increasing the concentration of $EuCl_3$ in complex solution [35,36], which probably results in a lower coverage with Pd nanoparticles and a lower H_2 gas response. Therefore the optimal concentration of Eu in ZnO:Eu columnar films in order to obtain the highest H_2 gas sensing characteristics/performances is about 0.05 at% Eu.

The dynamic H_2 gas responses of ZnO:Eu columnar films with different TA or RTA-treatments, as well as contents of Eu and functionalized with Pd measured to 100 ppm of hydrogen gas at an operating temperature of 250 ºC are presented in **Figure 10c**. All samples demonstrated a quite fast response to H_2 gas and complete recovery of signal after evacuation of hydrogen gas from the test chamber. The calculated response times for Eu1R650, Eu4R650, Eu1T650 and

Eu4T650 are ~22 s, 19 s, 3 s and 4 s, respectively, while the calculated recovery times are ~12 s, 19 s, 35 s and 25 s, respectively. In order to show the repeatability of the samples, the two consecutive pulses of hydrogen gas (100 ppm) were applied, showing a ~ 5% deviation in the response values in a short period between pulses (see **Figure 10d**). **Figure S9** shows the dynamic response of columnar ZnO films with about 0.05 at% Eu, where sample set Eu1T650 was subjected to Pd-functionalization versus 100 ppm of hydrogen at an operating temperature of 250 ºC. **Figure S10** shows the dynamic response of columnar ZnO films with about 0.20 at% Eu, marked as Eu4T650 and Pd-functionalized for 100 ppm of hydrogen at an operating temperature of 250 ºC, which clearly demonstrates sensor behavior of the developed new hybrid material. Thus, these results clearly prove the sensor behavior of the developed Pd-functionalized ZnO:Eu nanocolumnar films.

Figure S11 shows the H_2 gas response of Pd-functionalized ZnO:Eu columnar films to 100 ppm hydrogen versus treatment type, namely samples noted as Eu1(~0.05 at% Eu), Eu4(~0.2at% Eu) at an operating temperature of 200 °C and 250 °C, respectively. These samples were used with different types of treatment, namely **(a)-**as grown; RTA650-rapid thermal annealing; TA450, TA550, TA650-thermal annealing at 450, 550 and 650 °C, respectively. It can clearly be seen that for Eu-doped ZnO columnar films the most optimal concentration is ~0.05 at% followed by rapid thermal annealing at 650 °C (noted as Eu1_ RTA650).

The high selectivity and response of Pd-functionalized ZnO:Eu columnar films to hydrogen gas can be explained based on results obtained in previous works [24,26], where it was demonstrated that palladium oxide nanoparticles from the surface of ZnO grains, functionalized by the same method, are composed of PdO (88%) and PdO_2 (12%) [26]. Palladium oxide nanoparticles are a gas-sensing nanomaterial with a wide area of applications, namely in the conductometric/combustion-

type gas sensor applications [59,60], and has been extensively investigated as a promising hydrogen sensing nanomaterial, since its electrical resistance immediately increases by forming PdH_x under hydrogen atmosphere [59]. The use of palladium oxide instead of metallic palladium in gas sensing applications is more favorable due to the oxide protective layer that does not get irreversibly contaminated by gases presented in the atmosphere, as well as not damaged by the hydrogen embrittlement process on exposure to hydrogen gas [60].

3.5. Proposed gas sensing mechanism for nanocolumnar films.

In our case, the origin of the increased gas sensing performances is based on the selective modulation of the resistance in the ZnO/PdO heterojunction [61], because Pd ensure a low barrier energy for hydrogen gas dissociation and can act as an hydrogen gas sensitizer [61,62]. **Figure 11a** shows the energy band diagram of the *n*-ZnO/*p*-PdO interface. PdO is more suitable than palladium metal to trap electrons since it has a larger work function than Pd [63], thus the width of the depletion region is expected to be larger [63]. The work function (Φ) of palladium is ~5.12 eV, while the work function of PdO could reach values up to ~7.9 eV depending on the surface crystal orientation and its termination as found theoretically by Rogal *et al.* [63–65].

Under exposure to H_2 gas at temperatures higher than 101 °C, PdO oxide nanoparticles are reduced to Pd [66,67]:

$$PdO + H_2(g) \rightarrow Pd + H_2O(g) \quad (1)$$

The model energy band diagram of the formed *n*-ZnO/*p*-PdO interface is presented in **Figure 11b**. Further exposure to H_2 gas leads to direct dissolution of the hydrogen molecules in the octahedral sites of palladium, which changes its metallic state (palladium) into a hydride form, i.e. PdH_{xx}, where *xx* saturates at ~0.671 [68,69]:

$$xH^{+}(ad) + xe^{-} + Pd(s) \rightarrow PdH_{x}(s) \quad (2)$$

The work function of PdH_x was measured to be in the range of 3.2 – 5.27 eV according to previous works [70,71]. The formation of PdH_x with lower work function compared to ZnO:Eu facilitates the electrical charge carrier transfer from nanoparticles to zinc oxide and decreases the width of the electron depletion area, which essentially enhances the gas response and the selectivity to hydrogen H_2 gas (see **Figure 11c**) [26,61]. The role of Eu-doping in this study is to decrease the ZnO grain diameter of the columnar films (see **Figure 1** and **Figure 2**), which leads to a higher surface-to-volume ratio of the samples and thus to a higher coverage with Pd nanoparticles, as well as a higher coverage with oxygen species. The role of palladium nanodots in the enhancement of H_2 gas sensing abilities was attributed to an electrical sensitization mechanism (namely, forming of a space charge area around the nanodots, i.e., nano-scale Schottky barriers that narrow the conduction channel through ZnO:Eu columns) and chemical sensitization mechanism (catalytic dissociation of molecular oxygen by Pd nanodots, i.e., "spillover effect" which induce to electron withdrawal from the ZnO:Eu columns). Such characteristics of palladium as electrical conductivity and work function are known to be highly efficiently modulated by the adsorption of hydrogen gas. For details, see [24].[44]. Therefore, the surface functionalization efficiency is increased and a higher gas response can be obtained. Also, the presented XPS results of the Zn-2p core indicate the charge transfer between Eu^{3+} and Zn^{2+} which can lead to a higher concentration of free electrons and therefore to a higher coverage with oxygen species and hence a higher H_2 gas response [44]. At exposure of Pd/ZnO:Eu columns to H_2 gas the following reaction occurs:

$$2H \quad + O^{-}_{(ads)} \rightarrow H_2O_{(g)} + e^{-} \quad (3)$$

Another sensing mechanism could be possible and related to the kinetics of gas molecules. The high response to hydrogen gas could be also related to the smaller kinetic diameter of hydrogen gas.

4. CONCLUSIONS

In this work, the influence of the Eu content (in the range from 0.0 to ~0.2 at% Eu) on morphological, chemical, optical, structural and gas sensing properties of ZnO:Eu and Pd-functionalized ZnO:Eu columnar films with high crystallinity is reported for the first time. The doping with Eu (~0.05 at%) and surface functionalization with palladium nanoparticles were found to be highly efficient in order to achieve a high selectivity and excellent sensitivity to hydrogen gas at operating temperature of 200 – 300 ºC among other vapors of VOCs such as methane, ammonia, acetone, ethanol, *n*-butanol and 2-propanol and toxic or explosive gases. At an operating work temperature of 250 ºC a high gas response I_{gas}/I_{air} ~ 115 at 100 ppm H_2 was obtained, as well as a room temperature hydrogen sensor, which is essential for lowering the complexity, cost and size of the device by removing the need of a microheater and its circuit latter. Through density functional theory-based calculations, we found that due to H_2 gas interactions, the electronic properties of Pd-functionalized ZnO:Eu surface change with charge transfer from the surface to the molecule, which is also reflected in the electronic band shift and Fermi energy changes.

The obtained results on Pd-functionalized ZnO:Eu columnar films and supported with DFT calculations can be used for further improvement of synthesis parameters that can lead to the production of low-cost and highly efficient ZnO:Eu Pd-functionalized columnar films-based gas

sensors, selective to H_2 gas, even at room temperature, for personal, industrial, safety and environmental use.

■ ASSOCIATED CONTENT

Supporting Information: SEM images of ZnO:Eu films thermal annealed at 650 ºC in top-view and in sectional-view showing its thickness and columnar morphology. Compositional images measured by elemental EDX mapping at the microstructural level of columnar ZnO:Eu films thermal annealed at 650 ºC and EDX spectra. The overview spectra corresponding to ZnO:Eu thin films with increased Eu-doping concentration. DFT calculated bulk structure of ZnO and surface structures of two possible terminations of ZnO($10\bar{1}0$) surface, along with details of the surface energy calculations method. Modelled structures of Pd_n (n=1 to 9] cluster on the Eu doped ZnO($10\bar{1}0$) surface. Calculated adsorption energies and shortest Pd-Zn and Pd-O bond distances of the Pdn cluster with the first atomic layer of the ZnO slab for different Pdn/ZnO ($10\bar{1}0$) systems. Summary of the H_2 gas sensors based on pristine ZnO:Eu columnar films with different contents of Eu (0.00 at% Eu – Eu0; 0.05 at% Eu – Eu1; 0.10 at% Eu – Eu2; 0.15 at% Eu – Eu3 and 0.20 at% Eu – Eu4) to 100 ppm of different gases in air at an operating temperature of 350 ºC and at room temperature. The Supporting Information is available free of charge on the ACS Publications website at http://pubs.acs.org

■ AUTHOR INFORMATION

Corresponding Authors

†E-mails: thierry.pauporte@chimieparistech.psl.eu (Th.P.);

ra@tf.uni-kiel.de (R.A.) ; akmishra@ddn.upes.ac.in (A.K.M.) ; cristian.lupan@mib.utm.md (C.L.)

Notes

The authors declare no competing interest.

Author Contributions

The manuscript was written through contributions of all authors. All authors have given approval to the final version of the manuscript. ‡These authors contributed equally. C.L. and N.M. synthesized the Pd NPs -functionalized ZnO:Eu nanomaterial. C.L. adapted functionalization procedure for Pd NPs on ZnO:Eu. J.D., A.V., and F.F. realized all XPS experiments and data analysis. C.L., M.I.T. and N.M. adapted technological approach for material synthesis and integration/fabrication of the sensors for gas detection and SEM-EDX studies. C.L. and P.V. carried out the measurement of sensing properties of sensors based on such structures and analyzed all data. B.V. and C.L. realized all PL experiments and data analysis. C.L., Th.P. and P.V. realized all optical experiments and data analysis. C.L., V.P., Th.P., R.A., and A.V. analyzed the results, including experimental data and revised draft. R.K. and A.K.M. realized computational part and revised draft. C.L., V.P., R.K., A.K.M. and R.A. drafting the article. C.L., Th.P. and R.A. study conception and design, final approval of the version to be published. All authors reviewed the manuscript.

Funding Sources

NATO Science for Peace and Security Programme (SPS) under grant G5634 „Advanced Electro-Optical Chemical Sensors" AMOXES.

(DFG - Deutsche Forschungsgemeinschaft) under the schemes FOR 2093 and AD 183/18-1.

ACKNOWLEDGMENTS

C. Lupan gratefully acknowledges Kiel University, Functional Nanomaterials, Germany and PSL Université, Chimie-ParisTech IRCP, Paris, France for internship positions in 2018-2019 and TUM, Chisinau, Republic of Moldova, for constant support. C. Lupan would like to express special appreciation and thanks to Professor Trofim Viorel (TUM) as Thesis supervisor, for the encouragement, fruitful discussions on this work, patient guidance, and advice he has provided throughout time. This research was sponsored in part by the NATO Science for Peace and Security Programme (SPS) under grant G5634 „Advanced Electro-Optical Chemical Sensors" AMOXES. This investigation was partially supported by the German Research Foundation (DFG - Deutsche Forschungsgemeinschaft) under the schemes FOR 2093 and AD 183/18-1. The authors acknowledge Dr. David Santos-Carballal for fruitful discussions and proof-reading. A. K. Mishra acknowledges the computational facility of the University of Petroleum and Energy Studies, Dehradun. Katrin Brandenburg is acknowledged for her help in the final proof-reading of the manuscript.

■REFERENCES

(1) Stănoiu, A.; Simion, C. E.; Somăcescu, S. NO_2 Sensing Mechanism of ZnO-Eu_2O_3 Binary Oxide under Humid Air Conditions. *Sensors Actuators, B Chem.* **2013**, *186* (2), 687–694.

(2) Somacescu, S.; Dinescu, A.; Stanoiu, A.; Simion, C. E.; Calderon Moreno, J. M. Hydrothermal Synthesis of ZnO-Eu_2O_3 Binary Oxide with Straight Strips Morphology and Sensitivity to NO_2 Gas. *Mater. Lett.* **2012**, *89*, 219–222.

(3) Mishra, A. K.; Mishra, S. Tuning of Adsorption Energies of CO_2 and CH_4 in Borocarbonitrides $B_xC_yN_z$: A First-Principles Study. *J. Mol. Graph. Model.* **2019**, *93*, 107446.

(4) Khalediali dusti, R.; Mishra, A. K.; Barnoush, A. Atomic Defects in Monolayer Ordered Double Transition Metals Carbide ($Mo_2TiC_2T_x$) MXene and CO_2 Activation. *J. Mater. Chem. C* **2020**, *8*, 4771-4779.

(5) Zhao, C.; Li, Q.; Xie, Y.; Zhang, L.; Xiao, X.; Wang, D.; Jiao, Y.; Hurd Price, C. A.; Jiang, B.; Liu, J. Three-Dimensional Assemblies of Carbon Nitride Tubes as Nanoreactors for Enhanced Photocatalytic Hydrogen Production. *J. Mater. Chem. A* **2019**, *8* (1), 305–312.

(6) Liu, B.; Huo, L.; Si, R.; Liu, J.; Zhang, J. A General Method for Constructing Two-Dimensional Layered Mesoporous Mono- and Binary-Transition-Metal Nitride/Graphene as an Ultra-Efficient Support to Enhance Its Catalytic Activity and Durability for Electrocatalytic Application. *ACS Appl. Mater. Interfaces* **2016**, *8* (29), 18770–18787.

(7) Tian, H.; Huang, F.; Zhu, Y.; Liu, S.; Han, Y.; Jaroniec, M.; Yang, Q.; Liu, H.; Lu, G. Q. M.; Liu, J. The Development of Yolk–Shell-Structured Pd&ZnO@Carbon Submicroreactors with High Selectivity and Stability. *Adv. Funct. Mater.* **2018**, *28* (32), art. nr. 1801737.

(8) Zhang, Y. H.; Wang, C. N.; Gong, F. L.; Wang, P.; Guharoy, U.; Yang, C.; Zhang, H. L.; Fang, S. M.; Liu, J. Ultrathin Agaric-like ZnO with Pd Dopant for Aniline Sensor and DFT Investigation. *J. Hazard. Mater.* **2020**, *388*, art. nr. 122069.

(9) Hoppe, M.; Ababii, N.; Postica, V.; Lupan, O.; Polonskyi, O.; Schütt, F.; Kaps, S.; Sukhodub, L. F.; Sontea, V.; Strunskus, T.; Faupel, F.; Adelung, R. Sensors and Actuators B : Chemical (CuO-Cu_2O)/ZnO:Al Heterojunctions for Volatile Organic Compound Detection. *Sensors Actuators B. Chem.* **2018**, *255*, 1362–1375.

(10) Khaledialidusti, R.; Mishra, A. K.; Barnoush, A. Rheological Properties of Super Critical CO_2 with CuO:Multi-Scale Computational Modeling. *The J. Chem. Phys.* **2018**, *149* (22) art. nr. 224702.

(11) Ren, X.; Guo, M.; Li, H.; Li, C.; Yu, L.; Liu, J.; Yang, Q. Microenvironment Engineering of Ruthenium Nanoparticles Incorporated into Silica Nanoreactors for Enhanced Hydrogenations. *Angew. Chemie - Int. Ed.* **2019**, *58* (41), 14483–14488.

(12) Lupan, O.; Pauporté, T.; Viana, B.; Aschehoug, P.; Ahmadi, M.; Cuenya, B. R.; Rudzevich, Y.; Lin, Y.; Chow, L. Eu-Doped ZnO Nanowire Arrays Grown by Electrodeposition. *Appl. Surf. Sci.* **2013**, *282*, 782–788.

(13) Ahmed, S. M.; Szymanski, P.; El-Nadi, L. M.; El-Sayed, M. A. Energy-Transfer Efficiency in Eu-Doped ZnO Thin Films: The Effects of Oxidative Annealing on the Dynamics and the Intermediate Defect States. *ACS Appl. Mater. Interfaces* **2014**, *6* (3), 1765–1772.

(14) Chi Tsang, S.; Bulpitt, C. Rare Earth Oxide Sensors for Ethanol Analysis. *Sensors Actuators B Chem.* **1998**, *52* (3), 226–235.

(15) Hastir, A.; Kohli, N.; Singh, R. C. Comparative Study on Gas Sensing Properties of Rare Earth (Tb , Dy and Er) Doped ZnO Sensor. *J. Phys. Chem. Solids* **2017**, *105*, 23–34.

(16) Xu, X. Y.; Yan, B. Eu(Iii)-Functionalized ZnO@MOF Heterostructures: Integration of Pre-Concentration and Efficient Charge Transfer for the Fabrication of a Ppb-Level Sensing Platform for Volatile Aldehyde Gases in Vehicles. *J. Mater. Chem. A* **2017**, *5* (5), 2215–2223.

(17) Wang, M.; Huang, C.; Huang, Z.; Guo, W.; Huang, J.; He, H.; Wang, H.; Cao, Y.; Liu, Q.; Liang, J. Synthesis and Photoluminescence of Eu-Doped ZnO Microrods Prepared by Hydrothermal Method. *Opt. Mater. (Amst).* **2009**, *31* (10), 1502–1505.

(18) Geburt, S.; Lorke, M.; Da Rosa, A. L.; Frauenheim, T.; Röder, R.; Voss, T.; Kaiser, U.;

Heimbrodt, W.; Ronning, C. Intense Intrashell Luminescence of Eu-Doped Single ZnO Nanowires at Room Temperature by Implantation Created Eu-Oi Complexes. *Nano Lett.* **2014**, *14* (8), 4523–4528.

(19) Shahroosvand, H.; Ghorbani-Asl, M. Solution-Based Synthetic Strategies for Eu Doped ZnO Nanoparticle with Enhanced Red Photoluminescence. *J. Lumin.* **2013**, *144*, 223–229.

(20) Fonseca, A. F. V. da; Siqueira, R. L.; Landers, R.; Ferrari, J. L.; Marana, N. L.; Sambrano, J. R.; La Porta, F. de A.; Schiavon, M. A. A Theoretical and Experimental Investigation of Eu-Doped ZnO Nanorods and Its Application on Dye Sensitized Solar Cells. *J. Alloys Compd.* **2018**, *739*, 939–947.

(21) Postica, V.; Hölken, I.; Schneider, V.; Kaidas, V.; Polonskyi, O.; Cretu, V.; Tiginyanu, I.; Faupel, F.; Adelung, R.; Lupan, O. Multifunctional Device Based on ZnO:Fe Nanostructured Films with Enhanced UV and Ultra-Fast Ethanol Vapour Sensing. *Mater. Sci. Semicond. Process.* **2016**, *49*, 20–33.

(22) Kumar, V.; Kumar, V.; Som, S.; Duvenhage, M. M.; Ntwaeaborwa, O. M.; Swart, H. C. Effect of Eu Doping on the Photoluminescence Properties of ZnO Nanophosphors for Red Emission Applications. *Appl. Surf. Sci.* **2014**, *308*, 419–430.

(23) Zhou, R.; Zhao, Q.; Liu, K. K.; Lu, Y. J.; Dong, L.; Shan, C. X. Europium-Decorated ZnO Quantum Dots as a Fluorescent Sensor for the Detection of an Anthrax Biomarker. *J. Mater. Chem. C* **2017**, *5* (7), 1685–1691.

(24) Lupan, O.; Postica, V.; Labat, F.; Ciofini, I.; Pauporté, T.; Adelung, R. Ultra-Sensitive and Selective Hydrogen Nanosensor with Fast Response at Room Temperature Based on a Single Pd/ZnO Nanowire. *Sensors Actuators, B Chem.* **2018**, *254*, 1259–1270.

(25) Assadi, M.; Zhang, Y.; Zheng, R.-K.; Ringer, S.; Li, S. Structural and Electronic Properties of Eu- and Pd-Doped ZnO. *Nanoscale Res. Lett.* **2011**, *6* (1), art. nr. 357.

(26) Lupan, O.; Postica, V.; Hoppe, M.; Wolff, N.; Polonskyi, O.; Pauporté, T.; Viana, B.; Majérus, O.; Kienle, L.; Faupel, F.; Adelung, R. PdO/PdO_2 Functionalized ZnO:Pd Films for Lower Operating Temperature H2 Gas Sensing. *Nanoscale* **2018**, *10* (29), 14107–14127.

(27) Moulder, J. F.; Stickle, W. F.; Sobol, P. E.; Bomben, K. D. Handbook of Photoelectron Spectroscopy. *Phys. Electron. Inc., Eden Prairie, Minnesota* **1992**.

(28) Perdew, J. P.; Burke, K.; Ernzerhof, M. Generalized Gradient Approximation Made Simple. *Phys. Rev. Lett.* **1996**, *77* (18), 3865–3868.

(29) Kresse, G.; Joubert, D. From Ultrasoft Pseudopotentials to the Projector Augmented-Wave Method. *Phys. Rev. B* **1999**, *59* (3), 11–19.

(30) Kresse, G.; Furthmüller, J. Efficiency of Ab-Initio Total Energy Calculations for Metals and Semiconductors Using a Plane-Wave Basis Set. *Comput. Mater. Sci.* **1996**, *6* (1), 15–50.

(31) Monkhorst, H. J.; Pack, J. D. Special Points for Brillouin-Zone Integrations. *Phys. Rev. B* **1976**, *13* (4), 5188–5192.

(32) Methfessel, M.; Paxton, A. T. High-Precision Sampling for Brillouin-Zone Integration in Metals. *Phys. Rev. B* **1989**, *40* (6), 3616–3621.

(33) Grimme, S. Semiempirical GGA-Type Density Functional Constructed with a Long-Range Dispersion Correction. *Comput. Chem.* **2006**, *27*, 1787–1799.

(34) Henkelman, G.; Arnaldsson, A.; Jónsson, H. A Fast and Robust Algorithm for Bader Decomposition of Charge Density. *Comput. Mater. Sci.* **2006**, *36* (3), 354–360.

(35) Che, P.; Meng, J.; Guo, L. Oriented Growth and Luminescence of ZnO:Eu Films Prepared by Sol-Gel Process. *J. Lumin.* **2007**, *122–123* (1–2), 168–171.

(36) Korotcenkov, G.; Boris, I.; Cornet, A.; Rodriguez, J.; Cirera, A.; Golovanov, V.; Lychkovsky, Y.; Karkotsky, G. The Influence of Additives on Gas Sensing and Structural Properties of In_2O_3 -Based Ceramics. *Sensors Actuators, B Chem.* **2007**, *120* (2), 657–664.

(37) Kolmakov, A.; Klenov, D. O.; Lilach, Y.; Stemmer, S.; Moskovitst, M. Enhanced Gas Sensing by Individual SnO_2 Nanowires and Nanobelts Functionalized with Pd Catalyst Particles. *Nano Lett.* **2005**, *5* (4), 667–673.

(38) Sounart, T. L.; Liu, J.; Voigt, J. A.; Hsu, J. W. P.; Spoerke, E. D.; Tian, Z.; Jiang, Y. Sequential Nucleation and Growth of Complex Nanostructured Films. *Adv. Funct. Mater.* **2006**, *16* (3), 335–344.

(39) Sanchez Rayes, R. M.; Kumar, Y.; Cortes-Jácome, M. A.; Toledo Antonio, J. A.; Mathew, X.; Mathews, N. R. Effect of Eu Doping on the Physical, Photoluminescence, and Photocatalytic Characteristics of ZnO Thin Films Grown by Sol–Gel Method. *Phys. Status Solidi Appl. Mater. Sci.* **2017**, *214* (12), art. nr. 1700229.

(40) Ursaki, V. V.; Lupan, O. I.; Chow, L.; Tiginyanu, I. M.; Zalamai, V. V. Rapid Thermal Annealing Induced Change of the Mechanism of Multiphonon Resonant Raman Scattering from ZnO Nanorods. *Solid State Commun.* **2007**, *143* (8–9), 437–441.

(41) Swapna, R.; Kumar, M. C. S. Fabrication and Characterization of *n*-ZnO:Eu/*p*-ZnO:(Ag, N) Homojunction by Spray Pyrolysis. *Mater. Res. Bull.* **2014**, *49* (1), 44–49.

(42) Ivanova, T.; Harizanova, A.; Koutzarova, T.; Vertruyen, B. Study of ZnO Sol-Gel Films: Effect of Annealing. *Mater. Lett.* **2010**, *64* (10), 1147–1149.

(43) Rumble, J. R.; Bickham, D. M.; Powell, C. J. The NIST X-ray Photoelectron Spectroscopy Database. *Surf. Interface Anal.* **1992**, *19* (1–12), 241–246.

(44) Wang, X.; Xu, J.; Zhang, B.; Yu, H.; Wang, J.; Zhang, X.; Yu, J.; Li, Q. Signature of Intrinsic High-Temperature Ferromagnetism in Cobalt-Doped Zinc Oxide Nanocrystals. *Adv. Mater.* **2006**, *18* (18), 2476–2480.

(45) Zhong, J. B.; Li, J. Z.; Lu, Y.; He, X. Y.; Zeng, J.; Hu, W.; Shen, Y. C. Fabrication of Bi^{3+} -Doped ZnO with Enhanced Photocatalytic Performance. *Appl. Surf. Sci.* **2012**, *258* (11), 4929–4933.

(46) Hosseini, S. M.; Sarsari, I. A.; Kameli, P.; Salamati, H. Effect of Ag Doping on Structural, Optical, and Photocatalytic Properties of ZnO Nanoparticles. *J. Alloys Compd.* **2015**, *640*, 408–415.

(47) Lupan, O.; Pauporté, T.; Chow, L.; Viana, B.; Pellé, F.; Ono, L. K.; Roldan Cuenya, B.; Heinrich, H. Effects of Annealing on Properties of ZnO Thin Films Prepared by Electrochemical Deposition in Chloride Medium. *Appl. Surf. Sci.* **2010**, *256* (6), 1895–1907.

(48) Pessoni, H. V. S.; Maia, L. J. Q.; Franco, A. Eu-Doped ZnO Nanoparticles Prepared by the Combustion Reaction Method: Structural, Photoluminescence and Dielectric Characterization. *Mater. Sci. Semicond. Process.* **2015**, *30*, 135–141.

(49) Koao, L. F.; Dejene, F. B.; Kroon, R. E.; Swart, H. C. Effect of Eu^{3+} on the Structure, Morphology and Optical Properties of Flower-like ZnO Synthesized Using Chemical Bath Deposition. *J. Lumin.* **2014**, *147*, 85–89.

(50) Postica, V.; Hoppe, M.; Gröttrup, J.; Hayes, P.; Röbisch, V.; Smazna, D.; Adelung, R.; Viana, B.; Aschehoug, P.; Pauporté, T.; Lupan, O. Morphology Dependent UV Photoresponse of Sn-Doped ZnO Microstructures. *Solid State Sci.* **2017**, *71*, 75–86.

(51) Lupan, O.; Pauporté, T.; Tiginyanu, I. M.; Ursaki, V. V.; Şontea, V.; Ono, L. K.; Cuenya, B. R.; Chow, L. Comparative Study of Hydrothermal Treatment and Thermal Annealing Effects on the Properties of Electrodeposited Micro-Columnar ZnO Thin Films. *Thin Solid Films* **2011**, *519* (22), 7738–7749.

(52) Vanheusden, K.; Warren, W. L.; Seager, C. H.; Tallant, D. R.; Voigt, J. A.; Gnade, B. E. Mechanisms behind Green Photoluminescence in ZnO Phosphor Powders. *J. Appl. Phys.* **1996**, *79* (10), 7983–7990.

(53) Shishiyanu, S. T.; Lupan, O. I.; Monaico, E. V.; Ursaki, V. V.; Shishiyanu, T. S.; Tiginyanu, I. M. Photoluminescence of Chemical Bath Deposited ZnO:Al Films Treated by Rapid Thermal Annealing. *Thin Solid Films* **2005**, *488* (1–2), 15–19.

(54) Sawada, H.; Wang, R.; Sleight, A. W. An Electron Density Residual Study of Zinc Oxide. *J. Solid State Chem.* **1996**, *122* (1), 148–150.

(55) Jaffe, J. E.; Harrison, N. M.; Hess, A. C. Ab Initio Study of ZnO $(10\bar{1}0)$ Surface Relaxation. *Phys. Rev. B* **1994**, *49* (16), 11153–11158.

(56) Cooke, D. J.; Marmier, A.; Parker, S. C. Surface Structure of $(10\bar{1}0)$ and $(11\bar{2}0)$ Surfaces of ZnO with Density Functional Theory and Atomistic Simulation. *J. Phys. Chem. B* **2006**, *110* (15), 7985–7991.

(57) Wander, A.; Harrison, N. M. Ab-Initio Study of ZnO$(11\bar{2}0)$. *Surf. Sci.* **2000**, *468* (1–3), 851–855.

(58) Lupan, O.; Postica, V.; Adelung, R.; Labat, F.; Ciofini, I.; Schürmann, U.; Kienle, L.; Chow, L.; Viana, B.; Pauporté, T. Functionalized Pd/ZnO Nanowires for Nanosensors. *Phys. Status Solidi - Rapid Res. Lett.* **2018**, *12* (1), art. nr. 1700321.

(59) Cho, H. J.; Chen, V. T.; Qiao, S.; Koo, W. T.; Penner, R. M.; Kim, I. D. Pt-Functionalized PdO Nanowires for Room Temperature Hydrogen Gas Sensors. *ACS Sensors* **2018**, *3* (10), 2152–2158.

(60) Arora, K.; Puri, N. K. Electrophoretically Deposited Nanostructured PdO Thin Film for Room Temperature Amperometric H2 Sensing. *Vacuum* **2018**, *154*, 302–308.

(61) Kim, J. H.; Mirzaei, A.; Kim, H. W.; Kim, S. S. Pd Functionalization on ZnO Nanowires for Enhanced Sensitivity and Selectivity to Hydrogen Gas. *Sensors Actuators, B Chem.* **2019**, *297*, 126693-1 - 126693-9.

(62) Zhou, R.; Lin, X.; Xue, D.; Zong, F.; Zhang, J.; Duan, X.; Li, Q.; Wang, T. Enhanced H2 Gas Sensing Properties by Pd-Loaded Urchin-like $W_{18}O_{49}$ Hierarchical Nanostructures. *Sensors Actuators, B Chem.* **2018**, *260*, 900–907.

(63) Liu, Y.; Li, Q.; Zhang, J.; Sun, W.; Gao, S.; Shang, J. K. PdO Loaded TiO_2 Hollow Sphere Composite Photocatalyst with a High Photocatalytic Disinfection Efficiency on Bacteria. *Chem. Eng. J.* **2014**, *249*, 63–71.

(64) Rogal, J.; Reuter, K.; Scheffler, M. Thermodynamic Stability of PdO Surfaces. *Phys. Rev. B - Condens. Matter Mater. Phys.* **2004**, *69* (7), 075421-1 - 075421-8.

(65) Michaelson, H. B. The Work Function of the Elements and Its Periodicity. *J. Appl. Phys.* **1977**, *48* (11), 4729–4733.

(66) Chiang, Y. J.; Li, K. C.; Lin, Y. C.; Pan, F. M. A Mechanistic Study of Hydrogen Gas Sensing by PdO Nanoflake Thin Films at Temperatures below 250°C. *Phys. Chem. Chem. Phys.* **2015**, *17* (5), 3039–3049.

(67) Lee, Y. T.; Lee, J. M.; Kim, Y. J.; Joe, J. H.; Lee, W. Hydrogen Gas Sensing Properties of PdO Thin Films with Nano-Sized Cracks. *Nanotechnology* **2010**, *21* (16), 11–16.

(68) Dhall, S.; Kumar, M.; Bhatnagar, M.; Mehta, B. R. Dual Gas Sensing Properties of Graphene-Pd/SnO2 Composites for H2 and Ethanol: Role of Nanoparticles-Graphene Interface. *Int. J. Hydrogen Energy* **2018**, *43* (37), 17921–17927.

(69) Annanouch, F. E.; Haddi, Z.; Ling, M.; Di Maggio, F.; Vallejos, S.; Vilic, T.; Zhu, Y.; Shujah, T.; Umek, P.; Bittencourt, C.; Blackman, C.; Llobet, E. Aerosol-Assisted CVD-Grown PdO Nanoparticle-Decorated Tungsten Oxide Nanoneedles Extremely Sensitive and Selective to Hydrogen. *ACS Appl. Mater. Interfaces* **2016**, *8* (16), 10413–10421.

(70) Halas, S.; Durakiewicz, T. Is Work Function a Surface or a Bulk Property? *Vacuum* **2010**, *85* (4), 486–488.

(71) Singh, V.; Dhall, S.; Kaushal, A.; Mehta, B. R. Room Temperature Response and Enhanced Hydrogen Sensing in Size Selected Pd-C Core-Shell Nanoparticles: Role of Carbon Shell and Pd-C Interface. *Int. J. Hydrogen Energy* **2018**, *43* (2), 1025–1033.

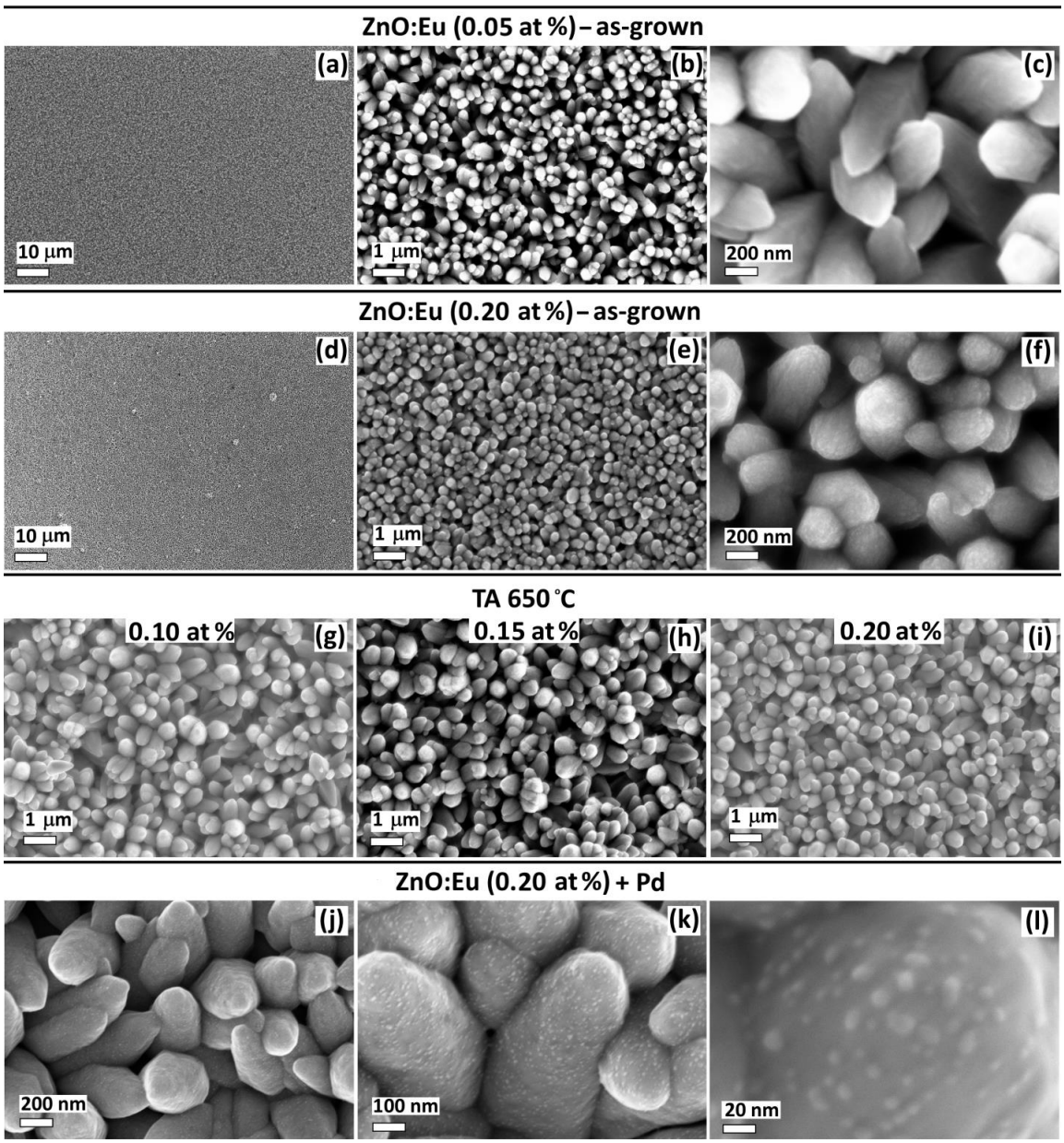

Figure 1. SEM images of as-grown ZnO:Eu columnar films by SCS approach with about: (a-c) 0.05 at% Eu; and (d-f) 0.2 at% Eu at different magnifications (from low to high starting from left to right). SEM images of TA-treated samples at 650 ºC for 2 h with the following content of Eu of about: (g) 0.1 at%; (h) 0.15 at%; and (i) 0.2 at%. SEM images of Pd-functionalized ZnO:Eu columnar films with about 0.2 at% Eu at different magnification: (j) low; (k) medium; and (l) high.

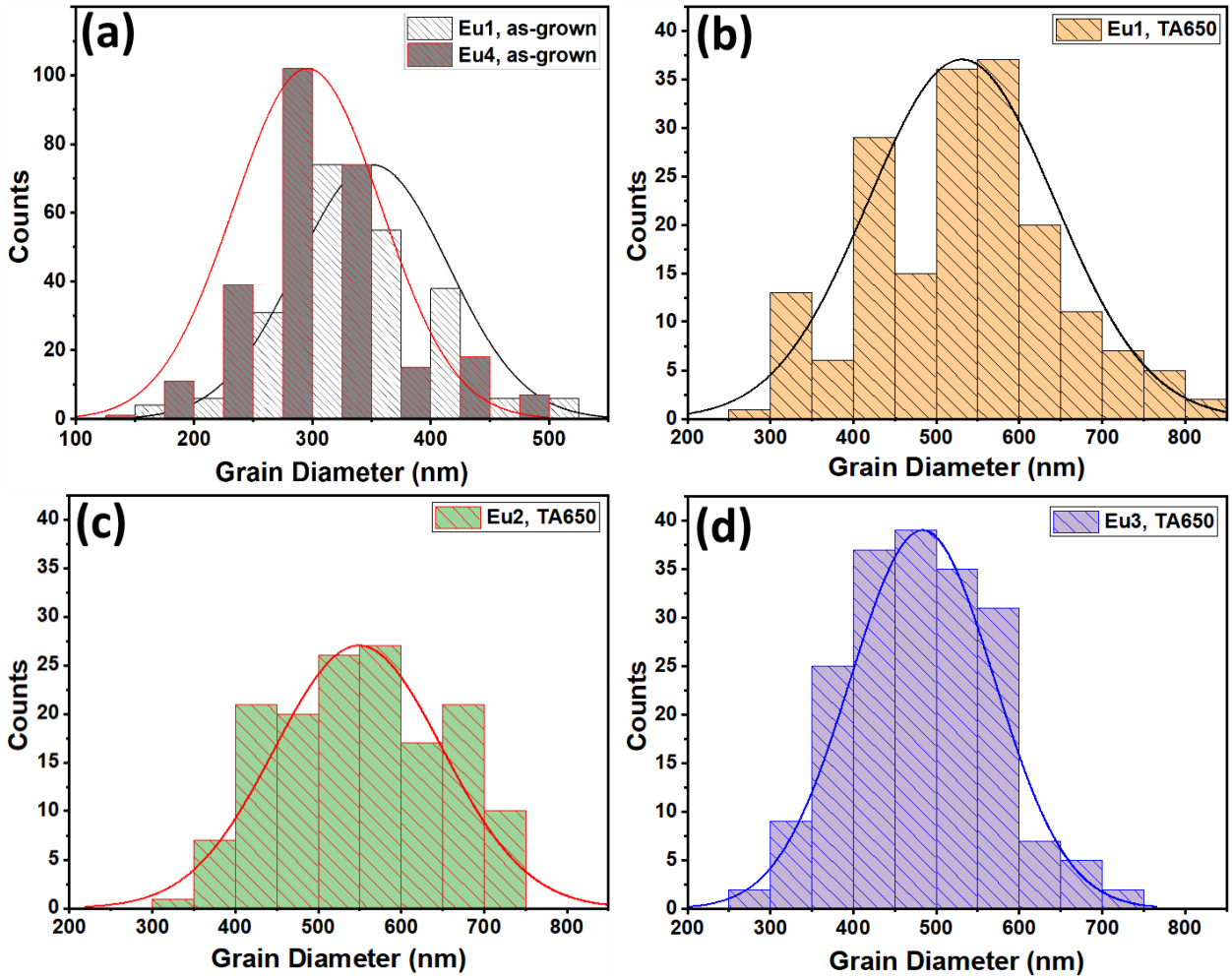

Figure 2. The grain diameter distribution for: (a) as-grown ZnO:Eu columnar films with about 0.05 at% Eu (Eu1) and 0.2 at% Eu (Eu4); and for TA-treated samples at 650 ºC with about (b) 0.05 at% Eu (noted as sample set Eu1); (c) 0.1 at% Eu (noted as Eu2); and (d) 0.15 at% Eu (noted as Eu3).

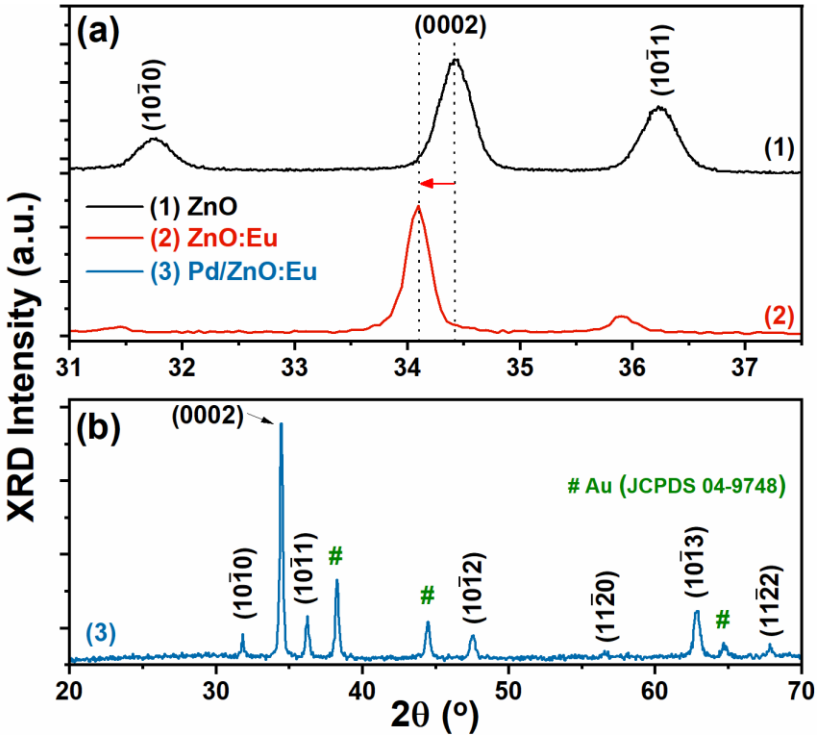

Figure 3. (a) Position of XRD (1 0 $\bar{1}$ 0), (0 0 0 2) and (1 0 $\bar{1}$ 1) diffraction peaks and intensity for ZnO and ZnO:Eu columnar films. (b) XRD diffraction pattern for Pd-functionalized ZnO:Eu columnar films annealed at 650 ºC with deposited Au contacts.

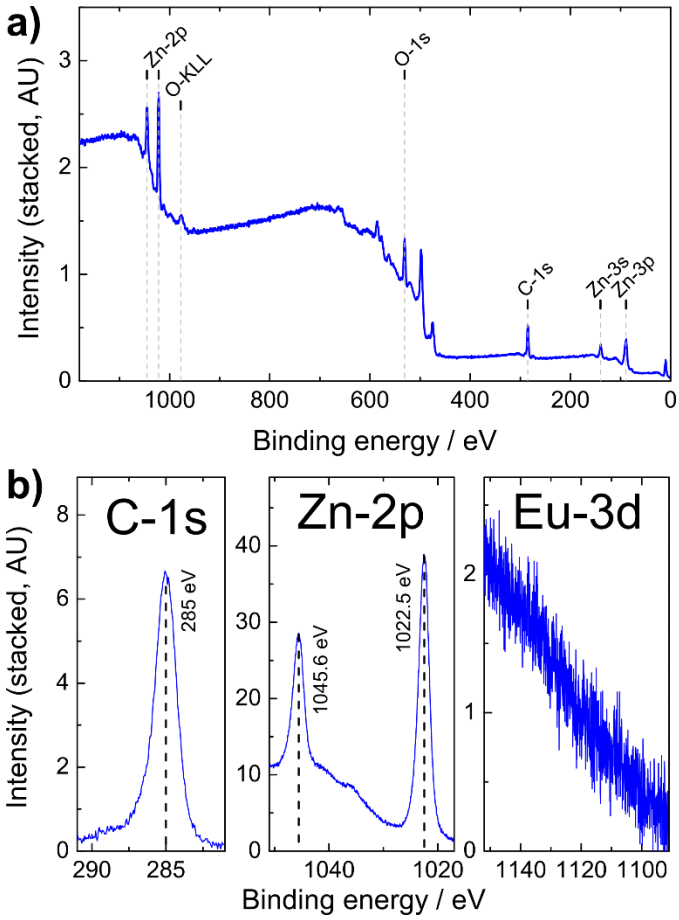

Figure 4. XPS spectra of a typical ZnO:Eu1 thin film annealed at 650 ºC in overview (a); and high resolution (b). The XPS investigation reveals the presence of Zn, O and C, while no clear signal correlating to Eu could be detected due to the low doping amount in the investigated sample set Eu1 and instrument detection limit.

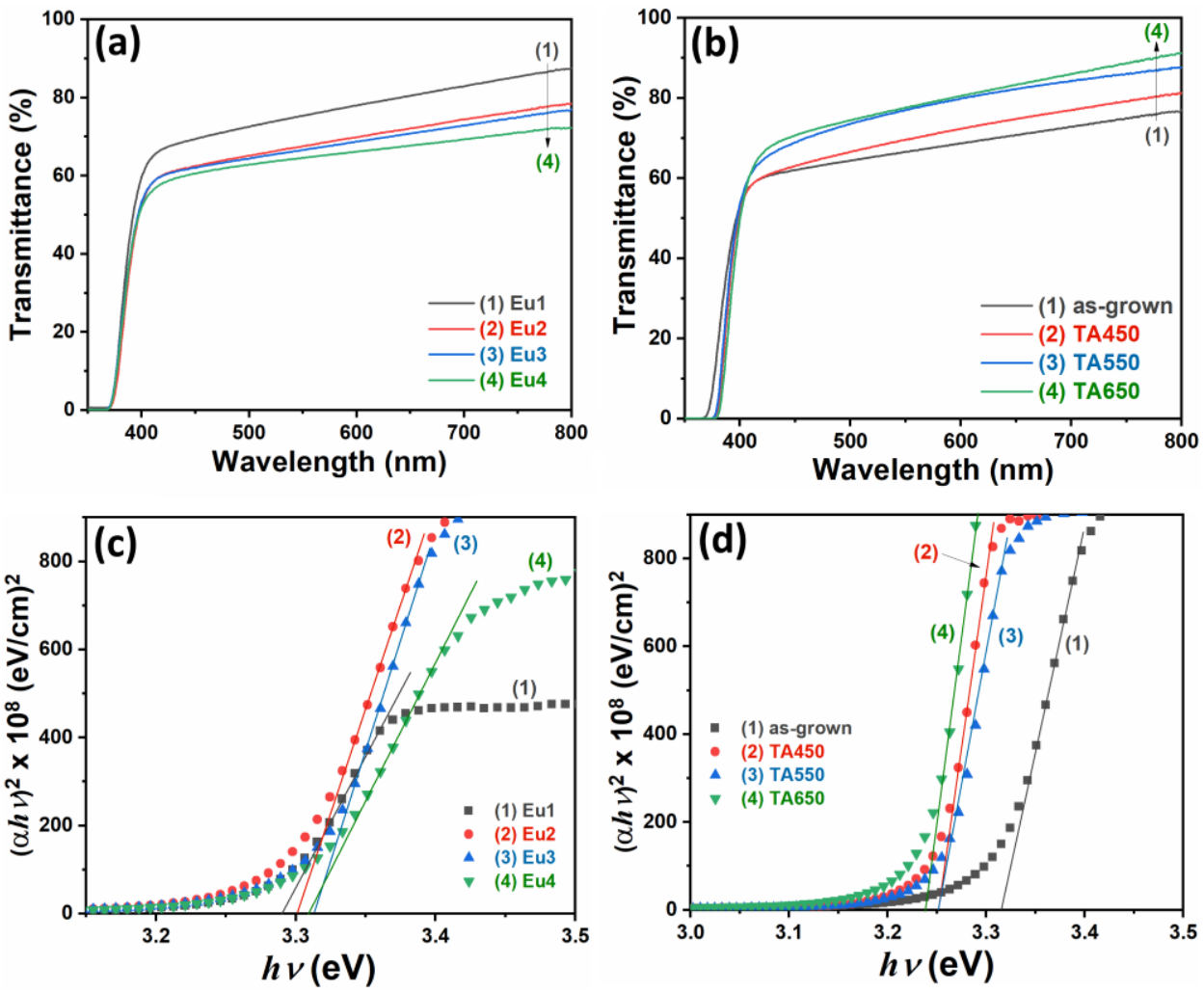

Figure 5. Transmission spectra of: (a) as-grown ZnO:Eu columnar films with different content of Eu; (b) ZnO:Eu columnar films with about 0.15 at% Eu TA-treated at different temperatures for 2 h. Plot of $(\alpha h\nu)^2$ *vs*. photon energy ($h\nu$) for: (c) as-grown ZnO:Eu columnar films with different content of Eu; (d) ZnO:Eu columnar films with about 0.15 at% Eu TA-treated at different temperatures for 2 h.

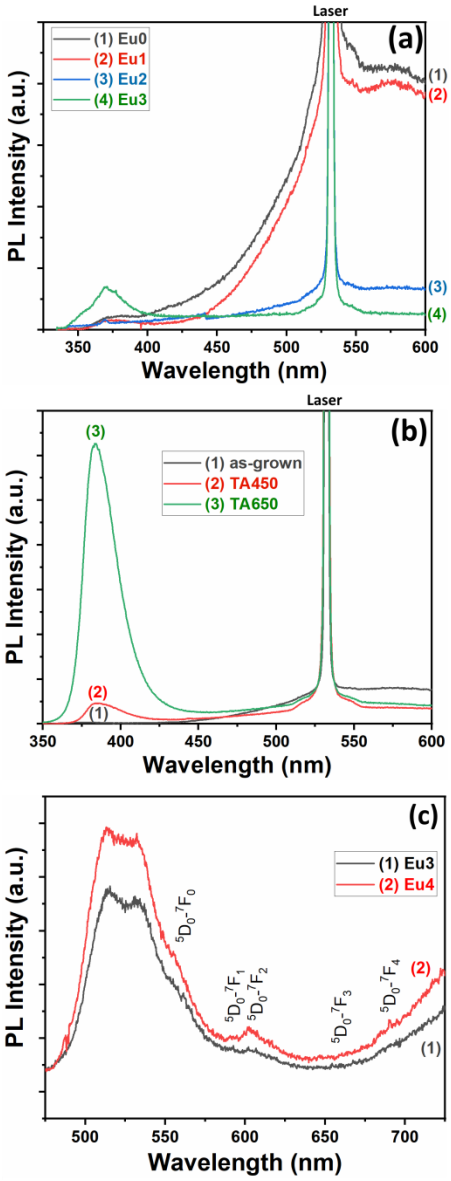

Figure 6. Room temperature PL spectra of: (a) as-grown ZnO:Eu columnar films with different content of Eu; (b) ZnO:Eu columnar films with about 0.10 at% Eu (Eu2) TA-treated at different temperatures for 2 h. The laser excitation wavelength was 266 nm and the line at 532 nm is due to the second order of the laser related to the grating and wavelength selection. (c) Visible emission spectrum at room temperature under pumping at 466 nm for ZnO:Eu columnar films TA-treated at 650 ºC for 2 h.

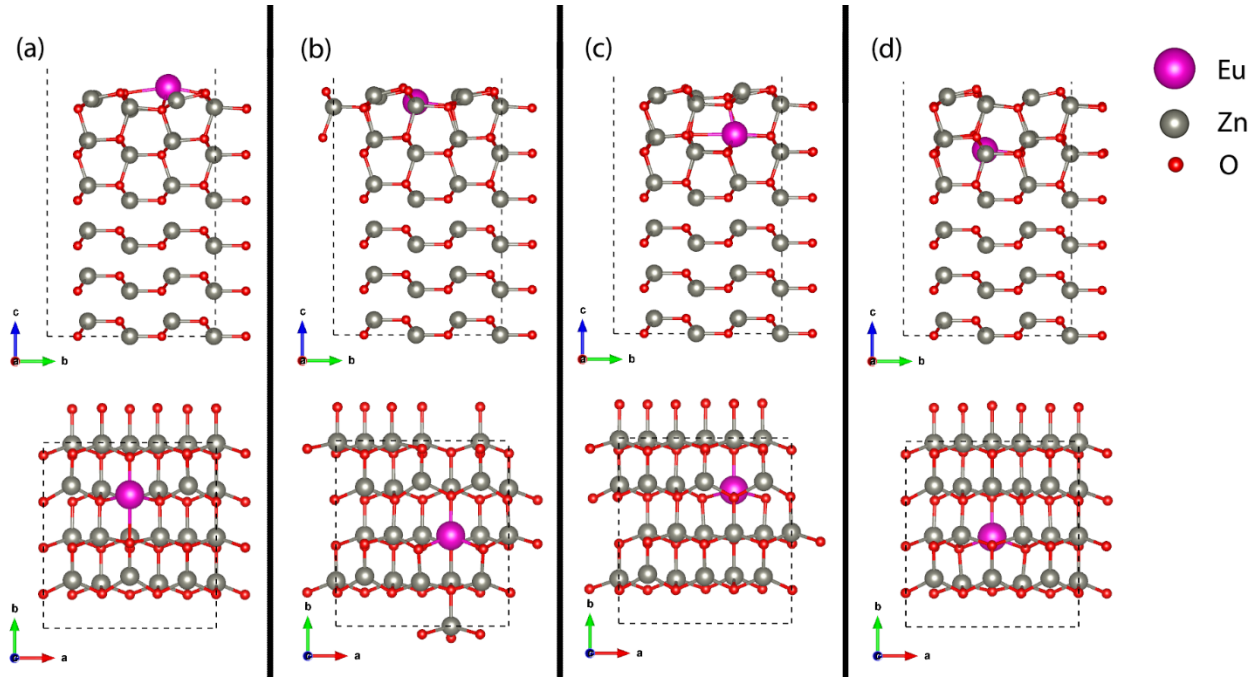

Figure 7. Eu atom doped in first layer top of ZnO(1 0 $\bar{1}$ 0) surface, substituting Zn atom (Fig a, b); Eu atom doped in second layer of ZnO(1 0 $\bar{1}$ 0) surface, substituting Zn atom (Fig b, c, d). Top and bottom panel shows top and side views of surface structures.

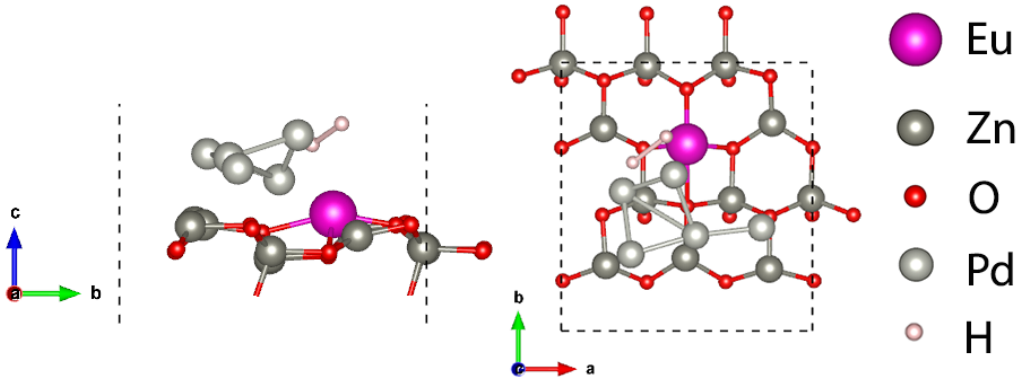

Figure 8. Top and side view of H_2 molecule interaction on Pd_5: Eu:ZnO(1 0 $\bar{1}$ 0) surface.

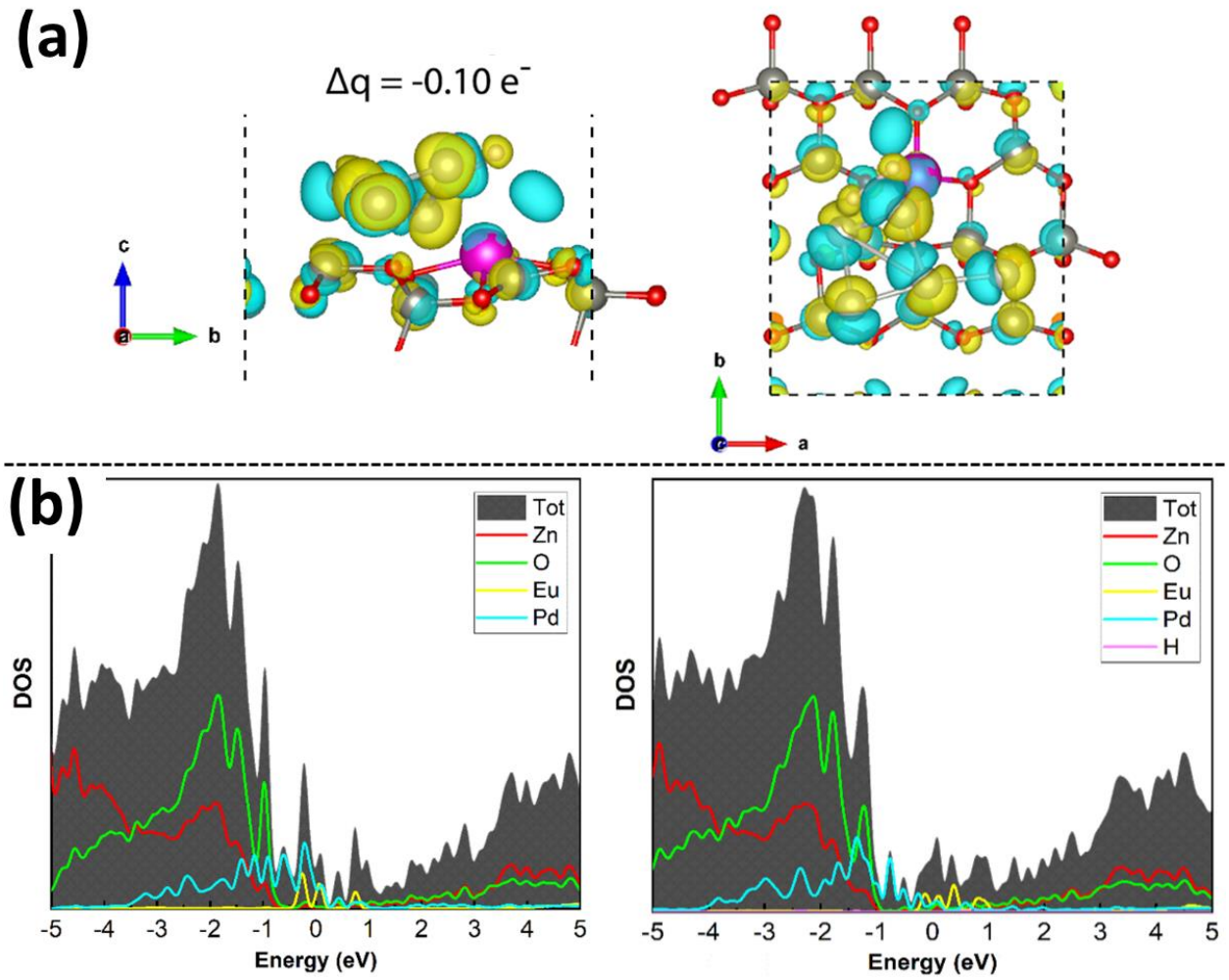

Figure 9. (a) Charge transfer analysis of H_2 molecule adsorption on Pd_5:Eu:ZnO(1 0 $\bar{1}$ 0) surface, (b) Density of states pdos of Pd_5:Eu:ZnO(1 0 $\bar{1}$ 0) surface (left) and pdos of H_2 molecule over Pd_5:Eu:ZnO(1 0 $\bar{1}$ 0) surface (right).

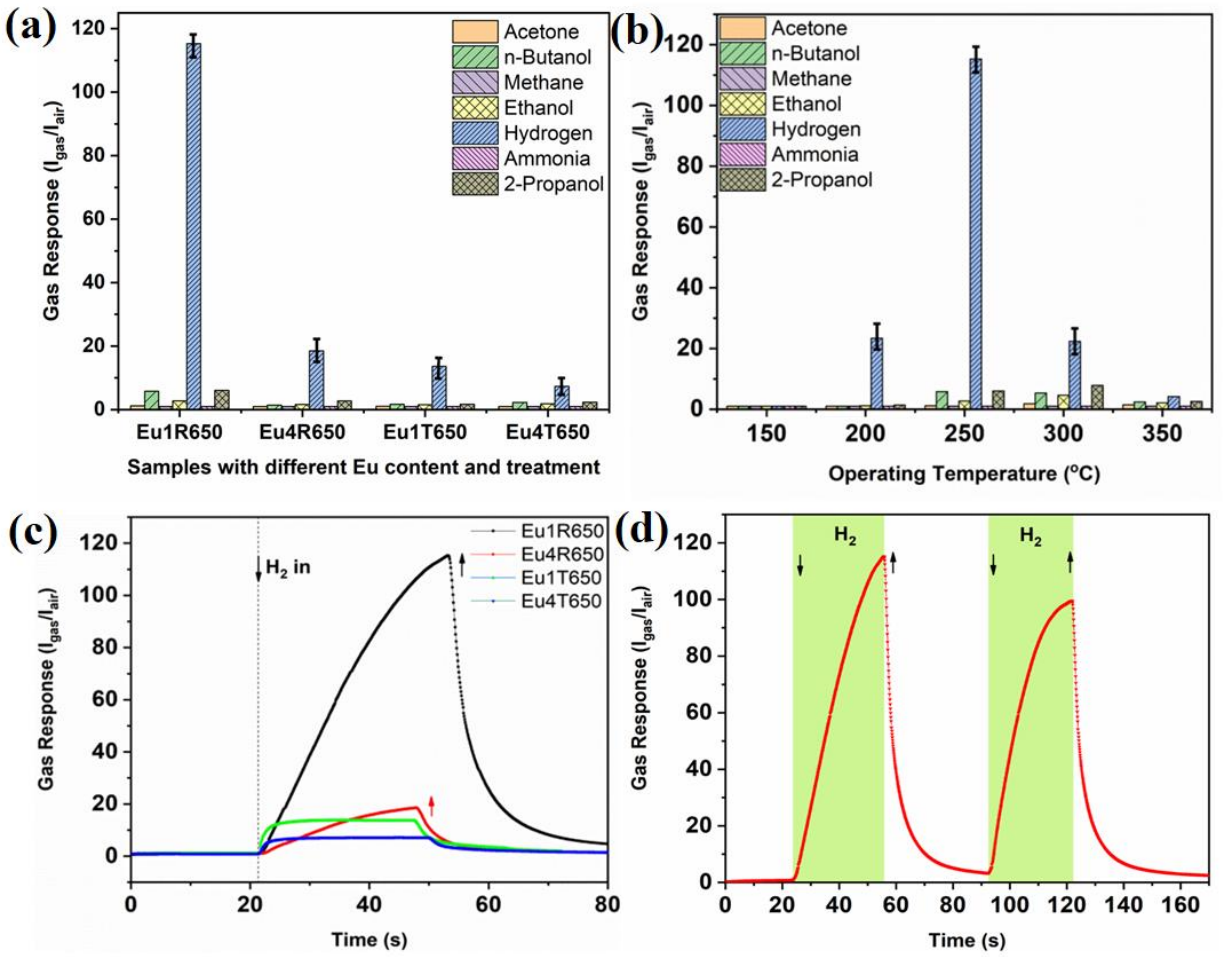

Figure 10. (a) Gas response of Pd-functionalized ZnO:Eu columnar films at operating temperature of 250 ºC to 100 ppm of different gases and vapors for sample sets: Eu1R650 – 0.05 at% Eu treated RTA at 650 ºC for 60 s; Eu4R650 – 0.2 at% Eu RTA-treated at 650 ºC for 60 s; Eu1T650 – 0.05 at% Eu treated TA at 650 ºC for 2 h; Eu4T650 – 0.2 at% Eu TA-treated at 650 ºC for 2 h. (b) Dependence of gas responses on operating temperature for Pd-functionalized ZnO:Eu columnar films with about 0.05 at% Eu and RTA-treated at 650 ºC for 60 s. (c) Dynamic responses to 100 ppm of H_2 gas for Pd-functionalized ZnO:Eu columnar films with different doping levels and types of annealing at operating temperature of 250 ºC. (d) Dynamic response to 100 ppm of H_2 for Pd-functionalized ZnO:Eu columnar films with about 0.05 at% Eu and RTA-treated at 650 ºC at operating temperature of 250 ºC to 100 ppm of H_2 gas.

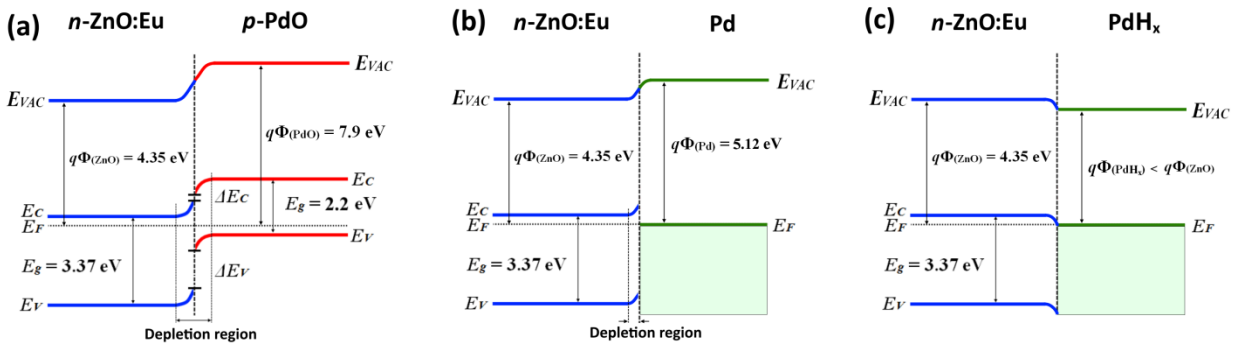

Figure 11. Model energy bands diagrams of: (a) *n*-ZnO:Eu/*p*-PdO; (b) *n*-ZnO:Eu/Pd; (c) *n*-ZnO:Eu/PdH_x in the case when work function of PdH_x is lower than for ZnO:Eu.

The table of contents entry (ToC)

High performance for detecting H_2 gas using ZnO:Eu columnar films functionalized with palladium nanoparticles (NPs) is reported and are attributed to synergetic effect of Pd NPs (7 – 14 nm) and Eu dopant atoms which enhance the catalytic properties. Experimental results indicate that Eu-doping with an optimal content about 0.05 – 0.1 at% along with Pd-functionalization of ZnO columns allows reducing the operating temperature of the H_2 gas sensor.

Pd-Functionalized ZnO:Eu Columnar Films for Room Temperature Hydrogen Gas Sensing: A Combined Experimental and Computational Approach

Cristian Lupan,[†,1] Rasoul Khaledialidusti,[2] Abhishek Kumar Mishra,[†,3,‡] Vasile Postica,[1,‡] Maik-Ivo Terasa,[4] Nicolae Magariu,[1] Thierry Pauporté,[†,5] Bruno Viana,[5] Jonas Drewes,[6] Alexander Vahl,[6] Franz Faupel,[6] Rainer Adelung[†,4]

ToC figure